Planarians Customize Their Stem Cell Responses Following Genotoxic Stress as a Function of Exposure Time and Regenerative State

Peer-reviewed author version

STEVENS, An-Sofie; WOUTERS, Annelies; PLOEM, Jan-Pieter; PIROTTE, Nicky; VAN ROTEN, Andromeda; WILLEMS, Maxime; Franken, Carmen; Koppen, Gudrun; HELLINGS, Niels; ARTOIS, Tom; PLUSQUIN, Michelle & SMEETS, Karen (2018)
Planarians Customize Their Stem Cell Responses Following Genotoxic Stress as a Function of Exposure Time and Regenerative State. In: TOXICOLOGICAL SCIENCES, 162(1), p. 251-263.

DOI: 10.1093/toxsci/kfx247
Handle: http://hdl.handle.net/1942/26279

Planarians customize their stem cell responses following genotoxic stress as a function of exposure time and regenerative state

An-Sofie Stevens*[1], Annelies Wouters*[1], Jan-Pieter Ploem*, Nicky Pirotte*, Andromeda Van Roten*, Maxime Willems[†‡], Niels Hellings[§], Carmen Franken[¶], Gudrun Koppen[¶], Tom Artois*, Michelle Plusquin[||], Karen Smeets*

*Zoology: Biodiversity and Toxicology, Centre for Environmental Sciences, Hasselt University, Agoralaan, building D, 3590 Diepenbeek, Belgium.

[†]Laboratory of Pharmaceutical Technology, Faculty of Pharmaceutical Sciences, Ghent University, 9000 Ghent, Belgium.

[‡]Laboratory of Environmental Toxicology & Aquatic Ecology, Ghent University, Jozef Plateaustraat 22, 9000 Ghent, Belgium.

[§]Biomedical Research Institute, Hasselt University, Agoralaan, building C, 3590 Diepenbeek, Belgium.

[¶]Environmental Risk and Health Unit, Flemish Institute for Technological Research (VITO), Boeretang 200, 2400 Mol, Belgium.

[||]Environmental Biology, Centre for Environmental Sciences, Hasselt University, Agoralaan, building D, 3590 Diepenbeek, Belgium.

[1]These authors contributed equally to this work

*Address correspondence to:

Karen Smeets. Zoology: Biodiversity and Toxicology, Centre for Environmental Sciences, Hasselt University, Agoralaan, Building D, 3590 Diepenbeek, Belgium. e-mail: karen.smeets@uhasselt.be; telephone: +3211268319

Running title: genotoxic stress in planarian stem cells

Abstract

Aiming to *in vivo* characterise the responses of pluripotent stem cells and regenerative tissues to carcinogenic stress, we employed the highly regenerative organism *Schmidtea mediterranea*. Its broad regenerative capacities are attributable to a large pool of pluripotent stem cells, which are considered key players in the lower vulnerability towards chemically-induced carcinogenesis observed in regenerative organisms. *S. mediterranea* is, therefore, an ideal model to study pluripotent stem cell responses with stem cells residing in their natural environment. Including microenvironmental alterations is important, as the surrounding niche influences the onset of oncogenic events. Both short (3 days) and long-term (17 days) exposures to the genotoxic carcinogen methyl methanesulphonate (50 μM) were evaluated during homeostasis and animal regeneration, two situations that render altered cellular niches. In both cases MMS-induced DNA damage was observed, which provoked a decrease in proliferation on the short term. The outcome of DNA damage responses following long-term exposure differed between homeostatic and regenerating animals. During regeneration, DNA repair systems were more easily activated than in animals in homeostasis, where apoptosis was an important outcome. Knockdown experiments confirmed the importance of DNA repair systems during carcinogenic exposure in regenerating animals as knockdown of *rad51* induced a stem cell-depleted phenotype, after regeneration was completed.

Key words

Planarians; Regeneration; Stem Cells; Genotoxicity; DNA Damage Response

1. Introduction

Stem cells possess strong defence systems against various stress factors such as carcinogenic compounds (Frosina, 2010; Vitale *et al.*, 2017). Being recruited into areas of tissue damage, they play a pivotal role in regeneration, delivering new cells to rebuild missing tissues. The downside is a possible transformation into cancer stem cells, creating immortal cells resistant to eradication and able to sustain tumour growth (Beck and Blanpain, 2013; Lambrou and Remboutsika, 2014). The behaviour of stem cells, defined by the balance between the amount of damage and the effectiveness of repair responses, is, therefore, crucial in directing the final outcome of cell proliferation during genotoxic insults towards tissue regeneration or tumour growth.

Stem cells have a diverse repertoire of stress defence mechanisms and responses towards DNA damage that vary throughout differentiation (Frosina, 2010; Mandal *et al.*, 2011; Nagaria *et al.*, 2013; Vitale *et al.*, 2017). Within the stem cell population, pluripotent and multipotent stem cells respond differently to stress factors. Wyles and colleagues showed that preferred DNA repair pathways or apoptotic sensitivity following DNA damage differ in both stem cell populations (Wyles *et al.*, 2014). Equally important is the direct microenvironment in which the stem cells reside, which influences intrinsic capacities such as stemness, differentiation and self-renewal (DeGregori, 2017; Lambrou and Remboutsika, 2014; Lane *et al.*, 2014). These capacities are coordinated by a variety of exogenous niche signals that are often neglected in an *in vitro* set-up. As cancer development is not only triggered by driving mutations but also by direct tissue changes, these factors are to be considered in toxicological studies (DeGregori, 2017).

Regenerative tissues are exceptionally resilient to carcinogenic compounds, making the entity of stem cells and their regenerative niche a useful research tool for

purposes that include, for example, potential drug target development (Oviedo and Beane, 2009). In the planarian *Schmidtea mediterranea,* a large pool of adult pluripotent stem cells underlies an extensive regenerative capacity (Aboobaker, 2011; Gentile *et al.*, 2011; Zhu and Pearson, 2016). Being a well-established stem cell model, it recently gained interest as a tool to investigate modes of action of toxicologically relevant compounds such as nanoparticles, neurotoxic drugs and carcinogenic compounds (Gentile *et al.*, 2011; Hagstrom *et al.*, 2015; Raffa *et al.*, 2013; Salvetti *et al.*, 2015). Their stem cell dynamics can be monitored *in vivo*, making these planarians extremely suitable to study responses of pluripotent stem cells to chemically-induced stressors in a realistic setting. At least two functionally distinct subtypes, sigma and zeta, can be distinguished within its stem cell pool, making it possible to monitor responses of different types of stem cells (van Wolfswinkel *et al.*, 2014; Wagner *et al.*, 2011; Zhu and Pearson, 2016). The sigma subclass most likely contains pluripotent stem cells, while the zeta class comprises cells that are in a more lineage-restricted state and that arise from cells of the sigma class (van Wolfswinkel *et al.*, 2014).

Previously, we reported that *S. mediterranea* responds to carcinogenic exposures by activating its stem cell system through alterations in proliferative responses (Plusquin *et al.*, 2012b; Stevens *et al.*, 2017). Both inhibition and stimulation of stem cell proliferation after exposure to respectively genotoxic and non-genotoxic carcinogens were observed (Stevens *et al.*, 2017). However, these responses rarely culminated in aberrant tissue formation, which is consistent with the assumption that growth abnormalities are formed to a lesser extent in regenerative animals and tissues, a correlation also found in mammals in the highly regenerative liver where carcinogen-

induced nodules are ‘easily’ remodelled into normal tissue (Farber, 1984; Levin, 2012; Oviedo and Beane, 2009; Pomerantz and Blau, 2013).

In this study, we exposed *S. mediterranea* to a strong genotoxic compound to characterise responses of its pluripotent stem cell system *in vivo*. We quantified DNA damaging effects, studied DNA damage response pathways and their outcomes, and looked at possible underlying mechanisms in situations with different microenvironments (DeGregori, 2017). More specifically, we compared responses during homeostasis and regeneration, the latter being a proliferation-stimulating environment. A second focus involved a comparison between effects on short and long-term exposure times.

2. Materials and Methods

2.1 Hazard information

Methyl methanesulphonate (MMS) is an alkylating agent and probable human carcinogen (IARC group 2a) (IARC, 1999).

2.2. Test organism and experimental design

Asexual strains of the freshwater planarian *Schmidtea mediterranea* were maintained in culture medium as described in Pirotte *et al.* (2015). All animals were starved 1 week before experiments, which is a common procedure in planarian research as food can influence results.

Experiments were performed during animal homeostasis and during regeneration (induced by amputation) to uncover regeneration-associated tumour suppression mechanisms. To synchronize their physiological state, the worms were cut transversally in front of the pharynx respectively 2 weeks (homeostatic animals) and immediately before (regenerating animals) exposure. As the animals regenerate

within 14 days, the homeostatic worms were synchronized and intact at the start of the experiments. For in-depth study of underlying mechanisms that are observed specifically during regeneration, only regenerating animals were used.

The animals were exposed to 50 µM MMS for 3 (short-term exposure) and 17 days (long-term exposure) in 6-well plates containing 4 ml of medium with/without the addition of 50 µM MMS (Cas # 66-27-3, Sigma-Aldrich, catalogue number 129925, purity 99%). Previous data indicated that 50 µM is a sublethal dosage that induces distinguishable effects (Stevens *et al.*, 2017). Medium was refreshed twice a week with freshly prepared MMS working solution (50 µM), a set-up previously optimized and compared to other exposure conditions (Stevens *et al.*, 2017). To prevent additional DNA damage which would interfere with our research question, DNA damage assessment and gene-expression measurements were performed on a stem cell-containing suspension (obtained with a cell dissociation protocol) instead of FACS-sorted cells.

2.3 Cell dissociation

To obtain a more uniform cell suspension containing stem cells, the planarian papain cell dissociation method based on Moritz *et al*. (2012) was used. In brief, the worms (at least 6 animals per sample) were incubated in 2% L-cysteine HCl (with 5 M NaOH until pH 7.0) for 2 minutes at room temperature and washed with CMFH (25.6 mM $NaH_2PO_4.2H_2O$, 142.8 mM NaCl, 102.1 mM KCl, 94.2 mM $NaHCO_3$, 0.1% BSA, 0.5% glucose, 15 mM Hepes, pH 7.2) before being cut into small pieces (in 250 µL CMFH). Papain solution (30 U/ml CMFH) with 1 mM L-cysteine was added for dissociation (1 hour at 26° C). DNase I (60 µg/ml CMFH) and Trypsin inhibitor, ovomucoid (1.5 mg/ml CMFH) were added and the pieces were triturated by pipetting. Cells were filtered (35 µm filter) to render a stem cell-containing fraction

from which larger cells are filtered out, washed with CMFH and collected through centrifugation for further processing.

2.4. Comet assay

DNA damage was assessed with the alkaline comet assay, based on Singh *et al.* (1988). We focused on responses in a fraction of smaller cells, among which stem cells and dividing stem cells, obtained after cell dissociation of 10 animals per sample. For each sample, 10 µl of the cell suspension was mixed with 120 µl 0.8% low melting point (LMP) agarose (GibcoBRL) in PBS, pipetted on a GelBond Film (Lonza), covered with a coverslip and placed at 4°C for 5 minutes to allow solidification. Two comet slides of each sample were made and considered as technical replicates. After removing coverslips, the slides were immersed in lysis solution (2.5 M NaCl, 0.1 M Na_2EDTA, 10 mM Tris, 1% Triton X-100, 10% DMSO, pH 10.0) overnight in the dark at 4°C to remove cellular membranes and proteins on DNA. After a washing step with PBS, slides were placed in an electrophoresis box filled with a cold alkaline solution (300 mM NaOH, 1 mM Na2EDTA, pH 13.0) and left there for 20 minutes to allow DNA unwinding. Electrophoresis was carried out at 20 V (0.8 V/cm over the platform) and 300 mA for 10 minutes at 4°C. The electrophoresis buffer was recirculated from anode to cathode using a peristaltic pump. After electrophoresis, slides were neutralized by a 5 minute wash in cold PBS, followed by a 5 minute wash in cold MilliQ water. DNA was stained with SYBR Gold Nucleic Acid Gel Stain (Invitrogen) and image analysis was performed using a Zeiss fluorescence microscope equipped with the semi-automatic Metafer 4 image analysis system (Metasystems) using 10x objective magnification. Measurements were made for ~ 300 cells per sample/condition. The relative amount of DNA damage (% DNA in the tail relatively to the total amount in the whole comet) was automatically assessed by

the system. Afterwards, falsely-scored nuclei or debris (artefacts) were manually eliminated based on visual inspection. Results were calculated as average of median % tail DNA of two (technical) replicated slides. The presented data are the result of two independent experiments.

2.5. Flow cytometry

Flow cytometry was used to analyse cell cycle distribution profiles. Six worms were collected per sample, and 3 samples were measured for each experimental condition following the protocol as described before (Pirotte *et al.*, 2015). Cells were obtained with the cell dissociation protocol, and were resuspended in CMFH with Calcein AM (Life technologies) (1:20000; 2 hours incubation at room temperature, shaking). Vybrant DyeCycle Ruby stain (Invitrogen) was then added for 30 minutes, cells were washed and resuspended in CMFH and flow cytometry analysis was performed using a BD FACSAria II Cell Sorter (BD Biosciences).

2.6. Gene expression

After the cell dissociation protocol with 6 worms per sample, total RNA was extracted from the stem cell-containing suspension with the NucleoSpin RNA XS kit (Macherey-Nagel) following the manufacturer's instructions. For the RNAi experiments of *pcna* and *rad51*, a phenol:chloroform protocol on a stem cell-containing pellet (6 worms per sample) was used as described previously (Pirotte *et al.*, 2015). RNA concentrations were assessed on the NanoDrop ND-1000 spectrophotometer (NanoDrop Technologies). Genomic DNA was removed with the Turbo DNA free kit (Ambion, Life Technologies). cDNA was synthesized using a Superscript III first-strand synthesis supermix (Invitrogen) following the manufacturer's instructions. SYBR Green (Applied Biosystems) chemistry-based

Real-Time PCR was performed in an optical 96-well plate using the ABI PRISM 7900 or 7500 (Applied Biosystems) under universal cycling conditions. The number of biological replicates used is indicated in the figure legends. PCR primers were designed using Primer3 software (Supplemental S1) (Untergasser *et al.*, 2012). The selection of potential reference genes was based on Plusquin *et al*. (2012a), after which the most stable reference genes during MMS exposure and per experimental set-up were determined by geNorm and GrayNorm analysis. Gene expression was performed with MIQE guidelines taken into account (Bustin *et al.*, 2009). Target sequences were based on (planarian) literature and were extracted from the *S. meditarranea* genome databases, i.e. SmedGD and/or Planmine (Brandl *et al.*, 2015; Robb *et al.*, 2015). For genes that were selected based on their function in other organisms the relevant human amino acid sequences were used for tblastn in the planarian databases SmedGD/Planmine. Details of the procedure are given in Supplemental S1.

2.7. Mitotic activity of stem cells

The mitotic activity of the stem cells was determined by immunostaining with an Histone H3 antibody (anti-phospho-histone H3 (Ser 10), biotin conjugate, Millipore, catalogue number 16-189), performed as described by Plusquin et al. (2012b). The total number of stem cells was normalized to the body area of the animals, which was determined prior fixation by taking 3 photos of each animal at the moment it stretches its body and determining the average body size using ImageJ (National Institutes of Health, Bethesda, MD, USA). Images were captured using a Nikon Eclipse 80i fluorescent microscope (Nikon Instruments, Melville, NY, USA). The number of biological replicates used is indicated in the figure legends.

2.8. Whole-mount TUNEL

Apoptotic cells were visualised using the ApopTag Red In Situ Apoptosis Detection Kit (Merck Millipore) following the manufacturer's instructions with some modifications based on Pellettieri *et al*. (2010) and Almuedo-Castillo *et al*. (2014). Briefly, after exposure, animals were fixed and permeabilized using 10% N-acetyl cysteine diluted in PBS (5 minutes, room temperature (RT)) and 4% formalin in PBST (0.3% Triton-X-100, 15 minutes, RT). Further permeabilization was performed using 20 µg/ml proteinase K in PBST (5 minutes, 37°C) and 4% formalin in PBST (15 minutes, RT). Samples were washed in PBST (5 minutes, RT) and transferred to a reduction solution consisting of 50 mM DTT, 1% Triton X-100 and 0.5% SDS dissolved in PBS (5 minutes, 37°C). Samples were washed in PBST (5 minutes, RT) and transferred to 1% SDS dissolved in PBS (15 minutes, RT). Two additional washing steps using PBST were performed before bleaching the worms with 6% H_2O_2 in PBST (overnight, RT). After bleaching, the samples were washed twice with PBST (5 minutes, RT) and exposed to 20 µl terminal transferase (TdT) enzyme diluted with reaction buffer (30% TdT enzyme/70% reaction buffer, overnight, 37°C). The next day samples were rinsed using stop/wash buffer (1 ml stop/wash buffer in 35 ml molecular H_2O, 5 minutes, RT) and PBST (1 minute, RT). The samples were then placed in 20 µl anti-DIG-Rhodamine diluted in blocking solution (47% anti-DIG-rhodamine/53% blocking solution) and incubated overnight at 4°C. Finally, the samples were washed using PBST-BSA (0.25%, 4 x 10 minutes and overnight, RT).

To determine the number of apoptotic cells/mm², the total number of fluorescent cells was normalized to the body size of the animals, which was determined using ImageJ (National Institutes of Health, Bethesda, MD, USA) by measuring the surface of the animals before sampling. Fluorescent images were acquired using a Zeiss LSM510

META (Carl Zeiss, Jena, Germany) mounted on an Axiovert 200M. A combined fluorescent image was created from the confocal stack images using ImageJ and the stained cells were counted using the ImageJ ITCN (Image-based Tool for Counting Nuclei) plug-in, with manual corrections. The number of biological replicates used is indicated in the figure legends.

2.9. Whole-mount immunohistochemistry

To visualise SMEDWI-1 protein levels, the same procedure as described previously was used, with the exception of using PBS instead of Holtfreter solution (Pirotte *et al.*, 2015). The primary antibody used was rabbit anti-SMEDWI-1, diluted 1:1500 and incubated during 18 hours at 4°C (Guo *et al.*, 2006). The secondary antibody (Alexa 568-conjugated goat anti-rabbit, Millipore, 1:500) was incubated during 16 hours at 4°C. Images were captured using a Zeiss LSM510 META (Carl Zeiss, Jena, Germany) mounted on an Axiovert 200M. Confocal stack images were merged to one combined image using ImageJ. The number of biological replicates used is indicated in the figure legends.

2.10. Whole-mount (fluorescent) in situ hybridization

Whole-mount in situ hybridization was performed as described previously with the slight modification of using PBS instead of Holtfreter solution (Pirotte *et al.*, 2015). Probes were synthesized using the DIG RNA labelling kit (Sp6/T7, Roche) following the manufacturer's instructions. *Smedwi-1* primers forward: 5' GTGACGCAGAGAAACGGAAG 3', reverse: 5' TTGGATTAGCCCCATCTTTG 3'; *NB.21.11e* primers forward: 5' GTGATTGCGTTCGCGTATATT 3', reverse: 5' ATTTATCCAGCGCGTCATATTC 3'. The number of biological replicates used is indicated in the figure legends.

Fluorescent in situ hybridization was performed based on previously described protocols (Currie *et al.*, 2016). In brief, mucus was removed with 5% N-acetyl cysteine in PBS (8 minutes) and animals were fixed in 4% formaldehyde/PBS (20 minutes). Samples were bleached overnight in 6% H_2O_2/MetOH solution and stored in methanol. After rehydratation and permeabilization of the tissue proteinase K (20 µg/ml in PBS, 6 minutes, RT), samples were incubated during 10 minutes in prehyb/PBST (0.3% Triton X-100) and then during 2 hours in prehyb (50% deionized formamide, 5X SSC, 0.1 mg/ml yeast tRNA 0.1 mg/ml heparin, 10 mM DTT, 1% Tween-20). The same *smedwi-1* probe as described above was synthesized, using a DNP-label (DNP-11-UTP, Perkin-Elmer), and was heated for 5 minutes at 80°C before use. Hybridization occurred overnight at 56°C, with 0.2 ng/µl probe diluted in hyb (prehyb + 10% dextran sulphate). Following a series of washing steps (wash hybe I: 50% formamide, 5X SSC and 0.1% Triton X-100; followed by a series of washing steps with a deceasing amount of wash hyb I and increasing amount of 2X SSC), samples were cooled down to room temperature and blocked during 2 hours in MABT (0.1% Tween-20, 0.1M maleic acid, 0.15M NaOH, 0.15M NaCl; pH 7.5) with 10% horse serum. An anti-DNP-HRP antibody (Perkin-Elmer) was incubated overnight, 1:1000 diluted in MABT with 10% horse serum. A series of MABT washing steps (4x 20 minutes) was followed by incubation with TSA-fluorescein labelling mix (Perkin-Elmer, diluted 1:250) during 40 minutes. Finally, samples were washed several times with MABT, fixed with 4% paraformaldehyde and mounted in glycerol. Images were captured using a Zeiss LSM510 META (Carl Zeiss, Jena, Germany) mounted on an Axiovert 200M. One confocal stack is visualized. The number of biological replicates used is indicated in the figure legends.

2.11. RNA interference

RNA interference (RNAi) was performed using double stranded RNA (dsRNA) probes for *smg1*, *ku80*, *rad51*, *pcna* and *bcl-2 antagonist*, generated by an *in vitro* transcription system (T7 RibomaxTM Express RNAi System, Promega) as indicated by the manufacturer's instructions. The primer and probe details are summarised in supplemental S2. The animals were injected with three 32.2 nl injections of 1 µg/µl dsRNA for 2 (*smg1, bcl-2 antagonist* and *pcna* for mitotic analysis) or 3 (*rad51*, *ku80* and *pcna*) consecutive days in the prepharyngeal part of the gut using the Nanoject II (Drummond Scientific). The non-RNAi group was injected with water. The following day animals were transversally cut in two and exposed to 0 and 50 µM MMS for 3 (phenotypic analysis), 10 (gene expression analysis) or 17 days (phenotypic, gene expression and mitotic analysis).

Visible, treatment-induced differences at the systemic level were studied in a phenotypic screening using a stereo microscope. Phenotypic effects of *smg1, pcna, rad51* and *ku80* knockdowns were monitored after short (3 days) and long-term (17 days) exposure to 0 and 50 µM MMS and compared with the phenotypes of water-injected, unexposed and MMS-exposed regenerating animals. The number of biological replicates used is indicated in the figure legends. Success of the RNAi effect on downregulation of the target genes was checked with real-time qPCR and ranged between 45%-60% for *bcl2*-antagonist, *smg1* and *ku80*. A range of > 80% was found for *pcna* and *rad51*.

2.12. Statistics

Categories (treatment/ regeneration) were statistically compared using one and two-way ANOVA. Main effects (effect of treatment, effect of regeneration, treatment*regeneration interaction effect) were considered when p-value < 0.05 and are discussed in the figure legends. Individual group comparisons (homeostatic non-

treated, homeostatic MMS-treated, regenerative non-treated and regenerative MMS-treated) were based on the Tukey-Kramer multiple comparison test. Normality was tested according to the normality test of Cramer-von Mises, Anderson-Darlin or a Shapiro-Wilk normality test. If the assumptions of normality were not met, a transformation was applied (log transformation for gene expression data). A nonparametric Kruskal-Wallis test was performed when data were not normally distributed after transformations. The statistical analyses were performed using R Statistical Software version 3.2.1 (Team, 2013). Principal component analysis was performed with R Statistical Software using the prcomp function; missing data was imputed using k-nearest neighbour method.

3. Results

DNA damage and subsequent damage responses were determined after *in vivo* exposures to the genotoxic compound MMS. Samples were filtered to remove large differentiated cells, resulting in a more uniform fraction of cells including stem cells.

Firstly, responses differed in homeostatic and regenerating animals, which were used to compare niche-dependent differences as exogenous cues differ in both scenarios to either maintain homeostasis or trigger a restorative response. Secondly, MMS effects differed depending on the exposure time: short and long-term effects are therefore discussed separately for all parameters.

3.1. MMS induces DNA damage in planarians is independent of exposure time and regenerative state

The presence of DNA breaks, determined with the alkaline comet assay, indicated a strong genotoxic MMS effect in all experimental settings. In all animals significantly elevated DNA damage was observed after short and long-term exposure to 50 µM

MMS, as compared with non-exposed control groups (Fig. 1). The proliferation-stimulating conditions of regenerating animals did not differently affect the magnitude of this damage.

3.2. The DNA damage response varies as a function of exposure time and regenerative state

Next, we investigated how the obtained DNA damage was further handled by focussing on the DNA damage response (DDR) pathway, which generally consists of sensors, signal transducers (such as *smg1*) and downstream effectors (such as *p53*), ultimately directing cell fate decisions (i.e. cell cycle arrest, apoptosis or altered differentiation) (Blanpain *et al.*, 2011; Sherman *et al.*, 2011; Stergiou and Hengartner, 2004). Activation was measured at the transcriptional level.

3.2.1. MMS decreases smg1 and p53 expression during short-term exposure

The effect of short-term MMS exposure on the transcript levels of *smg1*, which in planarians controls the initial response to injury to prevent hyperproliferation, was dependent on the physiological state of the animal. The only significant effect was found in regenerating animals, where *smg-1* expression was significantly downregulated due to exposure to MMS (p-value < 0.05) (Fig. 2a). A similar significant decrease (p-value < 0.01) was observed in the transcript levels of the planarian equivalent of the damage-effector *p53* following short-term MMS exposure (Fig. 2A). After long-term exposure, MMS increased the expression of *smg1* independent of the physiological state of the animal (overall MMS effect: p-value< 0.01). P*53* expression levels were not affected by MMS (Fig. 2a).

The importance of *smg1* and *p53* in activating the DDR pathway during genotoxic stress was further investigated by their knockdown via RNAi in regenerating animals,

as gene expression results were only significantly altered in this group. Compared with the water-injected controls, s*mg1(RNAi)* animals showed incomplete regeneration on the long term, namely failure to regenerate eyes in tail fragments (5/5) and smaller blastema sizes in heads (2/5) (Fig 2b). When combined with MMS exposure, phenotypic effects of *smg1* knockdown were less prominent in both head and tail fragments (e.g. successful eye development in exposed tails (6/6)). One water-injected head exposed to MMS displayed very vague eyes (1/6). When animals were cut into three parts, trunks failed to regenerate eyes when *smg1* was knocked down in both exposed (5/7) and non-exposed animals (4/6) (Supplemental S3). A knockdown of *p53* disabled hyperproliferative responses in regenerating organisms following long-term MMS exposure (Supplemental S4).

3.2.2. Time-dependent cell responses to MMS differ in a regenerative state

MMS-induced effects on the cell cycle

At the cellular level the amount of mitotic cells was significantly decreased in all animals after short-term MMS exposure compared with that of non-exposed animals (Fig. 3a). The expression of cell-cycle-regulating genes *cdc23* (G2/M transition in yeast and humans) (Sikorski *et al.*, 1993; Zhang *et al.*, 2011) and *cdc73* (negative regulation of G1/S-transition in humans) (Zhang *et al.*, 2006) was not affected following short-term MMS exposure (Fig. 3b).

WISH of *smedwi-1*, which is expressed in stem cells, showed that not only cells in the mitotic phase decreased, but that short-term exposure generally decreased the stem cell number (Guo *et al.*, 2006). The amount of *smedwi-1* positive cells declined in regenerating heads and tails, while trunks were not affected (Fig. 3c). *Smedwi-1* FISH on regenerating tails following 2 days of exposure indicated the same decrease

(5/7) (Fig. 3d). This result was however not confirmed with a FACS analysis, where no differences in the proportion of X1/X2/Xn cells were observed (Supplemental S5).

The expression levels of sigma subclass-associated genes (*soxP-1*, *soxP-2*, *soxB-1*, *fgfr-4*, *nlk1* and *pbx-1*) and zeta subclass-associated genes (*zfp-1*, *soxP-3*, *fgfr-1* and *p53*) (van Wolfswinkel *et al.*, 2014) were measured in a stem cell-containing fraction. Their expression did not show any significant differences following short-term exposure (supplemental S6) .

Long-term exposure to MMS significantly induced cell proliferation, but only in case animals were exposed during regeneration (p-value < 0.05) (Fig. 3a). In *smedwi-1* WISH staining patterns, the downregulation that was observed after short-term exposure was no longer visible following long-term exposure. Some variability was seen in exposed head fragments, with 3/7 displaying a reduced pattern (Fig. 3c). FACS on the contrary indicated a significant decrease of X1 cells in homeostatic animals following long-term exposure (Supplemental S5).

No significant fluctuations were detected in the stem cell subclasses-associated gene expression (Fig. 3e). Long-term MMS exposure increased the transcription level of *cdc23* (G2/M transition) in all animals (overall MMS effect p-value < 0.05), whereas *cdc73* (negative regulator G1/S transition) expression was not affected by MMS (Fig. 3b).

MMS-induced effects on stem cell differentiation

To investigate whether the altered stem cell numbers were accompanied by effects on early differentiation, we visualised the expression of *NB.21.1e* and measured the expression of *NB.32.1g*, both of which are early stem cell progeny markers (G0/G1/S-phase X2 cells) and *AGAT-1*, a late progeny marker (G0-phase X2-cells)

(Eisenhoffer *et al.*, 2008). Following short-term exposure, general patterns showed a downregulation in the expression of *NB.21.1e* only in exposed tails, while heads and trunks were unaffected by MMS (Fig. 4a). In contrast, gene expression levels of *NB.32.1g* were significantly doubled (p-value < 0.01) in regenerating animals under influence of MMS, while *AGAT-1* expression was not affected (Fig. 4b). Long-term exposure decreased *NB.21.11e* expression but only in tail fragments and some heads (4/7) (Fig. 4a). Long-term exposure did not significantly influence expression of *NB.32.1g* or *AGAT-1* (Fig. 4b).

Also SMEDWI-1 protein levels in the blastema were not altered following short or long-term exposure (Fig. 4c, data not shown).

MMS-induced apoptosis

To examine apoptotic cell death, we quantified apoptotic cells (TUNEL) and analysed the expression of both the prosurvival *bcl-2* gene and the proapoptotic *bcl2-3* gene, which is a *bcl-2* antagonist and will be further referred to as '*bcl-2* antagonist'.

Following short-term exposure, the number of apoptotic cells was unaffected by MMS exposure (Fig. 5a). Gene expression of apoptotic genes, however, was affected. In homeostatic animals a short-term exposure to MMS enhanced the expression of the *bcl-2* antagonist (p-value < 0.1), while it promoted survival in regenerating animals via the significantly-enhanced expression of *bcl2 (*p-value < 0.05*)* (Fig. 5b).

Long-term exposure caused an increasing trend in the number of apoptotic cells in homeostatic animals (p-value < 0.1), while MMS did not significantly alter the underlying expression patterns of *bcl-2* antagonist or *bcl-2* (Fig. 5a-b). No effects on apoptosis were seen in regenerating animals, which was functionally confirmed using

bcl-2 antagonist knockdowns. The MMS-induced increase in proliferation remained unaltered in exposed *bcl-2* antagonist knockdown animals (Fig. 5c).

3.3 MMS activates DNA repair in regenerating organisms

To assess the underlying mechanisms leading to the different cell fate decisions in homeostatic or regenerating animals, we focused on DNA repair mechanisms. As both single and double-strand breaks arise after MMS exposure, we measured transcript levels of planarian equivalents of *rad51* (homologous recombination, HR) and *ku80* and *ku70* (non-homologous end-joining, NHEJ) to assess double-strand break repair. As indicator of single-strand repair *pcna* was measured. This gene participates in many repair pathways including base-excision-repair (BER), which is important for the repair of N-methylated bases induced by MMS and is also a key factor in DNA synthesis and cell cycle regulation (Ensminger *et al.*, 2014; Fortini and Dogliotti, 2007; Savio *et al.*, 1998). For nucleotide excision repair (NER), expression of the damage-recognition gene *XPA* was measured (Sugitani *et al.*, 2016).

Following short-term MMS exposure, only *ku70* was significantly decreased (p-value < 0.05), and this only in regenerating animals (Fig. 6a). Several of the other genes (*pcna*, *rad51*) were increased due to the regeneration process (main effect of regeneration p-value <0.05 for *rad51* p-value < 0.01 for *pcna*), but unaffected to the MMS exposure (data not shown). After long-term exposure, the expression of both *pcna* and *ku80* significantly (p-value < 0.05) increased when MMS was administered during regeneration (Fig. 6a). Also in this time period, no significant effects were observed in homeostatic animals.

Knocking down the repair genes *pcna* and *rad51* confirmed the need of DNA repair activation when animals are exposed during regeneration. A stem cell-depleted

phenotype was observed starting from 17 (*pcna*) or 14 (*rad51*) days of exposure, while non-MMS-treated animals were not affected at this time point (Fig. 6b). A similar phenotype was sometimes observed in non-exposed knockdown animals, but only at a later time point or not in all replicates (data not shown). *Rad51* exposed heads died sooner than the other exposed knockdowns. In case of *ku80* knockdown, no aberrant phenotype was detected (Fig. 6b). Knockdown of *pcna* also converted the MMS-induced proliferation (long-term) into a hypoproliferative response, confirming the stem cell-depleted phenotype (Fig. 6c). Knockdown of *rad51* in regenerating tails led to a decreased amount of proliferating stem cells, but only when combined with MMS exposure (Fig 6c.).

To better understand and localize the observed transcriptional effects in regenerating animals, a Principal Component Analysis (PCA) was performed to relate the observed gene expression patterns to responses of the stem cell subclasses separately (Fig. 6d). Following long-term exposure in regenerating animals, sigma-associated genes clustered together with the prosurvival *bcl-2* gene and DNA repair genes, except for *rad51*. *Zfp-1*, a zeta-exclusive gene, grouped with the proapoptotic *bcl-2* antagonist, while other zeta-associated genes were more widespread. The zeta-associated *p53* and *sox* gene clustered together with a sigma-associated *sox* gene (Fig. 6d). To further relate DNA repair with sigma and zeta, their gene expression was measured in a knockdown situation of *pcna* and *rad51* (Fig. 6e). Following 10 days of exposure—before the phenotypes arose—sigma (represented by *soxP-1* and *soxP-2*) and zeta (represented by *zfp-1*) gene expression was measured in a stem cell- containing fraction (Fig. 6e). Knockdown of *pcna* and *rad51* in regenerating heads decreased both subclass-associated genes in both a control

and exposed situation (Fig. 6e). Similar patterns were observed in regenerating tail fragments (supplemental S7).

4. Discussion

Having a prominent role in development, tissue homeostasis and repair, stem cells possess superior stress response mechanisms compared with their differentiated counterparts (Rocha *et al.*, 2013; Vitale *et al.*, 2017). Insights in their toxicological defence mechanisms will help to understand and address toxicity issues during, for example, (cancer) drug development or regenerative medicine. Both a low apoptotic threshold as well as an enhanced DNA repair activity— primarily homologous recombination and non-homologous end-joining— are generally proposed as main defence strategies of stem cells upon genotoxic stress (Blanpain *et al.*, 2011; Fan *et al.*, 2011; Insinga *et al.*, 2014; Mandal *et al.*, 2011; Wyles *et al.*, 2014). These repair responses can differ depending on the direct environment in which the stem cells reside e.g. during embryogenesis as compared with later life stages (Udroiu and Sgura, 2016). A recent study emphasizes on incorporating microenvironmental changes in cancer risk models, stating for example that the altered microenvironment in aged tissue increases cancer incidence (DeGregori, 2017), Aiming to characterise responses in pluripotent stem cells to carcinogenic stress in variable microenvironments, we used the planarian *S. mediterranea* as an *in vivo* system, with stem cells residing in their natural environment during genotoxic exposure. We compared stem cell responses to the genotoxic carcinogen MMS during homeostasis and regeneration, both characterised by distinct stem cell dynamics and corresponding cellular niches. While homeostatic animals represent a stem cell steady-state situation, regeneration mimics development by triggering massive proliferation, leading to an increased niche competition among stem cells.

We focused on the stem cell's short-term and long-term DNA damage responses, time points based on previously characterised MMS-induced changes in stem cell dynamics as indicated in the experimental set-up (Stevens *et al.*, 2017). Short-term effects will be discussed in light of the long-term consequences, as distinct responses depending on the regenerative status of the animal were mainly observed following long-term exposure.

Our results show a strong increase in DNA damage irrespective of the physiological state of the animal and exposure time (Fig. 1). Stem cell responses, however, did differ. *S. mediterranea's* stem cells reacted with a cell cycle arrest following short-term exposure (Fig. 3a), a response also observed in more differentiated cells (Fox and Fox, 1967; Stergiou and Hengartner, 2004). This can be a direct result of the alkylating effect of MMS which is known to slow down S-phase progression via effects on replication forks, by blocking new origin firing, or by checkpoint activation and as such temporarily decreases the number of mitotic cells (Fox and Fox, 1967; Lee *et al.*, 2007; Merrick *et al.*, 2004; Song, 2005; Stergiou and Hengartner, 2004). The unaltered expression levels of the cell cycle regulating genes *cdc23* and *cdc73* (Fig. 3b) also favour this hypothesis.

Notwithstanding the decreased proliferation and a concurrently general decrease of stem cells (reduced *smedwi-1* expression) in regenerating heads and tails (Fig. 3c-d), animals were still able to regenerate successfully as no aberrant regeneration phenotypes were observed on the long term. A comparable level of early differentiation processes was achieved despite lower amounts of stem cells, indicating that regeneration is prioritized and can override carcinogenic processes (Fig. 4). This is also demonstrated by an induction of hyperproliferation following

long-term exposure in regenerating animals, which does not precede malignancy as is usually the case in carcinogenic processes (Fig. 3a). In case of knockdown of repair-associated genes, the implicated stem cell-depleted phenotype only arose after the regeneration process took place (Fig. 6b).

The observed proliferation arrest following short-term exposure is equally present in homeostatic and regenerating animals, but the propagation of the damage signal as well as downstream cell fate decisions vary depending on the physiological state of the animal (Fig. 2a, Fig. 5b). Expression of DNA damage transducer *smg1* and effector *p53* significantly decreases in exposed regenerating animals, fluctuations that were not observed during homeostasis (Fig. 2a). Although classically being assigned a tumour suppressor function, p53 in planarians has been shown to have a role as tumour suppressor (vertebrate *p53*) as well as modulating stem cell self-renewal (vertebrate *p63)* (Pearson and Sanchez Alvarado, 2010). Its downregulation upon genotoxic stress favours its role in self-renewal and coincides with earlier described findings of a downregulation in the presence of dsDNA breaks (induced by *rad51* RNAi) (Peiris *et al.*, 2016). In other organisms, it has been found that P53 exerts a different role in stem cells than in differentiated cells, as differentiation is accompanied by a switch towards more p53-dependent processes in contrast to p53 inhibition in a more potent cell state (Insinga *et al.*, 2014; Vitale *et al.*, 2017). The observed combination of decreased *p53* and increased *bcl-2* to promote cell survival was also described in other tissue-specific adult stem cells such as colon stem cells following irradiation (Fig. 2a, 5b) (Insinga *et al.*, 2014). While a long-term MMS exposure did not significantly affect *p53* expression, *p53* silencing during regeneration disabled MMS-induced hyperproliferation, which is consistent with the role of *p53* in re-activating self-renewal as described above (Supplemental S4). It is

possible that during genotoxicity p53 functions as a cellular fate switch towards self-renewal in stem cells. Also *smg1* expression decreased in regenerating exposed animals, indicating that its described role to avoid hyperproliferation is of lesser importance in a genotoxic context (Fig. 2). Knockdown experiments confirmed its minor role as phenotypes were less prominent in exposed animals compared with unexposed animals (Fig. 2b). Nevertheless, it has to be stated that phenotypes in the control situation were also affected to a lesser extent than described in literature; differences that can be due to a different injection-scheme (Gonzalez-Estevez *et al.*, 2012).

Following long-term MMS exposure, differences between homeostatic and regenerative animals become even more apparent. A niche with more proliferating cells (regeneration) directs cellular fate outcomes towards DNA repair instead of apoptosis (homeostatic animals). Based on literature and our data, we suspect that the unequal amount of proliferating stem cells, the direct cellular environment, and the functional aim of the stem cells at that moment (i.e. to regenerate or not), underlie this difference in outcomes. Measuring both DNA repair and apoptosis, the latter was found to be more pronounced in homeostatic animals (Fig. 5, 6a). On the transcriptional level, we saw a significant activation of several DNA repair genes (*ku80* and *pcna*) during regeneration (Fig. 6a). Possibly, repair mechanisms enable regenerating organisms to promote cell survival instead of cell death, which is necessary to support successful regeneration. In this case, possible BER-induced DNA breaks can be repaired by either homologous recombination (*rad51*) or non-homologous end-joining (*ku70-ku80*) during replication (Ensminger *et al.*, 2014). To further study the functional relevance of these DNA repair mechanisms during regeneration, they were knocked down. *Pcna* and *rad51* but not *ku80* knockdown led

to a stem cell-depleted phenotype, a decreased amount of mitotic cells and a decreased expression of sigma and zeta-associated genes in exposed *pcna* and *rad51* knockdown animals (Fig. 6b,c,e). As the choice between both repair pathways partly depends on the cell cycle stage, and homologous recombination being mainly active during the S-phase, this coincides with the observed cell cycle effects (Mao *et al.*, 2008). The activation of repair mechanisms is not only niche-dependent, but also seems to vary between stem cell subtypes. The expression of sigma-associated genes clustered with DNA repair genes, while *zfp-1* —a zeta exclusive gene— was associated with the pro-apoptotic *bcl-2* antagonist (Fig. 6d). Data are based on a correlation analysis of a limited set of genes and not single-cell measurements, but the link between *zfp-1* and the *bcl-2* antagonist is an important indication since *zfp-1* is specifically linked to the zeta-subclass and an early progeny state (Abnave *et al.*, 2017; van Wolfswinkel *et al.*, 2014). The observed correlation also corresponds to findings in other systems, for instance how pluripotent versus multipotent stem cells activate distinct repair systems upon genotoxic stress in mammalian cells (Wyles *et al.*, 2014). Measuring sigma and zeta-associated genes following DNA repair knockdown in an exposed situation did, however, not show any decisive differences between their expression, making further research on single-cell level necessary (Fig. 6e).

In conclusion, while short-term reactions upon genotoxic exposure provoke a proliferation arrest, pluripotent stem cells can recover from this induced DNA damage and successfully regenerate an entire organism. As opposed to stem cells in other systems, we do not observe any malignancy, implicating an active repair programme. Depending on the microenvironment and needs of the organism (homeostatic versus regenerating), responses toggle between apoptosis and DNA repair, with *p53* as a

probable regulator of the stem cell's self-renewal switch. Our study confirms the importance of measuring toxicological responses in different conditions, as responses varied as a function of changing cellular environments and needs. Future work will pinpoint involved factors and how they are relevant in defining the outcome of either a malignant or restorative process.

Funding information

This work was supported by Bijzonder OnderzoeksFonds of Hasselt university [grant number BOF08G01]; Hasselt University tUL-impulsfinanciering [project toxicology] Fonds voor Wetenschappelijk Onderzoek [grant number 1522015N and PhD grant number R6411 to Annelies Wouters] and Agentschap voor Innovatie door Wetenschap en Technologie [grant number 101442 to An-Sofie Stevens and OZM grant number 100631 to Maxime Willems].

Acknowledgements

The authors thank Natascha Steffanie and Ria Vanderspikken for their skilful technical assistance. Nikki Watson is acknowledged for her help with some linguistical questions.

References

Abnave, P., Aboukhatwa, E., Kosaka, N., Thompson, J., Hill, M. A., and Aboobaker, A. A. (2017). Epithelial-mesenchymal transition transcription factors control pluripotent adult stem cell migration in vivo in planarians. *Development* 144(19), 3440-3453.

Aboobaker, A. A. (2011). Planarian stem cells: a simple paradigm for regeneration. *Trends Cell Biol.* 21(5), 304-11.

Almuedo-Castillo, M., Crespo-Yanez, X., Seebeck, F., Bartscherer, K., Salo, E., and Adell, T. (2014). JNK controls the onset of mitosis in planarian stem cells and triggers apoptotic cell death required for regeneration and remodeling. *PLoS Genet* 10(6), e1004400.

Beck, B., and Blanpain, C. (2013). Unravelling cancer stem cell potential. *Nat. Rev. Cancer* 13(10), 727-738 (Perspectives).

Blanpain, C., Mohrin, M., Sotiropoulou, P. A., and Passegue, E. (2011). DNA-damage response in tissue-specific and cancer stem cells. *Cell Stem Cell* 8(1), 16-29.

Brandl, H., Moon, H., Vila-Farre, M., Liu, S. Y., Henry, I., and Rink, J. C. (2015). PlanMine - a mineable resource of planarian biology and biodiversity. *Nucleic Acids Res* doi: 10.1093/nar/gkv1148.

Bustin, S. A., Benes, V., Garson, J. A., Hellemans, J., Huggett, J., Kubista, M., Mueller, R., Nolan, T., Pfaffl, M. W., Shipley, G. L.*, et al.* (2009). The MIQE guidelines: minimum information for publication of quantitative real-time PCR experiments. *Clin. Chem.* 55(4), 611-22.

Currie, K. W., Brown, D. D. R., Zhu, S., Xu, C., Voisin, V., Bader, G. D., and Pearson, B. J. (2016). HOX gene complement and expression in the planarian Schmidtea mediterranea. *EvoDevo* 7, 7.

DeGregori, J. (2017). Connecting cancer to its causes requires incorporation of effects on tissue microenvironments. *Cancer research* doi: 10.1158/0008-5472.can-17-1207.

Ensminger, M., Iloff, L., Ebel, C., Nikolova, T., Kaina, B., and Lbrich, M. (2014). DNA breaks and chromosomal aberrations arise when replication meets base excision repair. *J Cell Biol* 206(1), 29-43.

Fan, J., Robert, C., Jang, Y. Y., Liu, H., Sharkis, S., Baylin, S. B., and Rassool, F. V. (2011). Human induced pluripotent cells resemble embryonic stem cells demonstrating enhanced levels of DNA repair and efficacy of nonhomologous end-joining. *Mutat Res* 713(1-2), 8-17.

Farber, E. (1984). Pre-cancerous steps in carcinogenesis. Their physiological adaptive nature. *Biochim Biophys Acta* 738(4), 171-80.

Fortini, P., and Dogliotti, E. (2007). Base damage and single-strand break repair: mechanisms and functional significance of short- and long-patch repair subpathways. *DNA Repair (Amst)* 6(4), 398-409.

Fox, M., and Fox, B. W. (1967). Effect of methyl methanesulfonate on the growth of P388 lymphoma cells in vitro and on their rate of progress through the cell cycle. *Cancer research* 27(10), 1805-12.

Frosina, G. (2010). The bright and the dark sides of DNA repair in stem cells. *J. Biomed. Biotechnol.* 2010, 845396.

Gentile, L., Cebrià, F., and Bartscherer, K. (2011). The planarian flatworm: an in vivo model for stem cell biology and nervous system regeneration. *Dis. Model. Mech.* 4(1), 12-19.

Gonzalez-Estevez, C., Felix, D. A., Smith, M. D., Paps, J., Morley, S. J., James, V., Sharp, T. V., and Aboobaker, A. A. (2012). SMG-1 and mTORC1 act antagonistically to regulate response to injury and growth in planarians. *PLoS Genet* 8(3), e1002619.

Guo, T., Peters, A. H., and Newmark, P. A. (2006). A Bruno-like gene is required for stem cell maintenance in planarians. *Dev. Cell* 11(2), 159-69.

Hagstrom, D., Cochet-Escartin, O., Zhang, S., Khuu, C., and Collins, E. M. (2015). Freshwater Planarians as an Alternative Animal Model for Neurotoxicology. *Toxicol. Sci.* 147(1), 270-85.

IARC (1999). Re-evaluation of some organic chemicals, hydrazine and hydrogen peroxide. Proceedings of the IARC Working Group on the Evaluation of Carcinogenic Risks to Humans. Lyon, France, 17-24 February 1998. *IARC Monogr. Eval. Carcinog. Risks Hum.* 71 Pt 1, 1-315.

Insinga, A., Cicalese, A., and Pelicci, P. G. (2014). DNA damage response in adult stem cells. *Blood Cells Mol. Dis.* 52(4), 147-151.

Lambrou, G. I., and Remboutsika, E. (2014). Proliferation versus regeneration: the good, the bad and the ugly. *Front. Physiol.* 5, 10.

Lane, S. W., Williams, D. A., and Watt, F. M. (2014). Modulating the stem cell niche for tissue regeneration. *Nat Biotech* 32(8), 795-803 (Research).

Lee, M. Y., Kim, M. A., Kim, H. J., Bae, Y. S., Park, J. I., Kwak, J. Y., Chung, J. H., and Yun, J. (2007). Alkylating agent methyl methanesulfonate (MMS) induces a wave of global protein hyperacetylation: implications in cancer cell death. *Biochem Biophys Res Commun* 360(2), 483-9.

Levin, M. (2012). Morphogenetic fields in embryogenesis, regeneration, and cancer: non-local control of complex patterning. *BioSyst.* 109(3), 243-61.

Mandal, P. K., Blanpain, C., and Rossi, D. J. (2011). DNA damage response in adult stem cells: pathways and consequences. *Nat. Rev. Mol. Cell Biol.* 12(3), 198-202.

Mao, Z., Bozzella, M., Seluanov, A., and Gorbunova, V. (2008). DNA repair by nonhomologous end joining and homologous recombination during cell cycle in human cells. *Cell cycle (Georgetown, Tex.)* 7(18), 2902-6.

Merrick, C. J., Jackson, D., and Diffley, J. F. (2004). Visualization of altered replication dynamics after DNA damage in human cells. *The Journal of biological chemistry* 279(19), 20067-75.

Moritz, S., Stockle, F., Ortmeier, C., Schmitz, H., Rodriguez-Esteban, G., Key, G., and Gentile, L. (2012). Heterogeneity of planarian stem cells in the S/G2/M phase. *Int J Dev Biol* 56(1-3), 117-25.

Nagaria, P., Robert, C., and Rassool, F. V. (2013). DNA double-strand break response in stem cells: Mechanisms to maintain genomic integrity. *Biochimica et Biophysica Acta (BBA) - General Subjects* 1830(2), 2345-2353.

Oviedo, N. J., and Beane, W. S. (2009). Regeneration: The origin of cancer or a possible cure? *Semin Cell Dev Biol* 20(5), 557-64.

Pearson, B. J., and Sanchez Alvarado, A. (2010). A planarian p53 homolog regulates proliferation and self-renewal in adult stem cell lineages. *Development* 137(2), 213-21.

Peiris, T. H., Ramirez, D., Barghouth, P. G., Ofoha, U., Davidian, D., Weckerle, F., and Oviedo, N. J. (2016). Regional signals in the planarian body guide stem cell fate in the presence of DNA instability. *Development* doi: 10.1242/dev.131318.

Pellettieri, J., Fitzgerald, P., Watanabe, S., Mancuso, J., Green, D. R., and Sánchez Alvarado, A. (2010). Cell death and tissue remodeling in planarian regeneration. *Dev Biol* 338(1), 76-85.

Pirotte, N., Stevens, A.-S., Fraguas, S., Plusquin, M., Van Roten, A., Van Belleghem, F., Paesen, R., Ameloot, M., Cebri, #xe0*, et al.* (2015). Reactive Oxygen Species in Planarian Regeneration: An Upstream Necessity for Correct Patterning and Brain Formation. *Oxid. Med. Cell. Longev.* 2015, 19.

Plusquin, M., DeGheselle, O., Cuypers, A., Geerdens, E., Van Roten, A., Artois, T., and Smeets, K. (2012a). Reference genes for qPCR assays in toxic metal and salinity stress in two flatworm model organisms. *Ecotoxicology* 21(2), 475-84.

Plusquin, M., Stevens, A. S., Van Belleghem, F., Degheselle, O., Van Roten, A., Vroonen, J., Blust, R., Cuypers, A., Artois, T., and Smeets, K. (2012b). Physiological and molecular characterisation of cadmium stress in Schmidtea mediterranea. *Int J Dev Biol* 56(1-3), 183-91.

Pomerantz, J. H., and Blau, H. M. (2013). Tumor suppressors: enhancers or suppressors of regeneration? *Development* 140(12), 2502-12.

Raffa, R. B., Danah, J., Tallarida, C. S., Zimmerman, C., Gill, G., Baron, S. J., and Rawls, S. M. (2013). Potential of a planarian model to study certain aspects of anti-Parkinsonism drugs. *Advances in Parkinson's Disease* Vol.02No.03, 5.

Robb, S. M. C., Gotting, K., Ross, E., and Sánchez Alvarado, A. (2015). SmedGD 2.0: The Schmidtea mediterranea genome database. *Genesis* doi: 10.1002/dvg.22872, n/a-n/a.

Rocha, C. R. R., Lerner, L. K., Okamoto, O. K., Marchetto, M. C., and Menck, C. F. M. (2013). The role of DNA repair in the pluripotency and differentiation of human stem cells. *Mutation Research/Reviews in Mutation Research* 752(1), 25-35.

Salvetti, A., Rossi, L., Iacopetti, P., Li, X., Nitti, S., Pellegrino, T., Mattoli, V., Golberg, D., and Ciofani, G. (2015). In vivo biocompatibility of boron nitride nanotubes: effects on stem cell biology and tissue regeneration in planarians. *Nanomedicine (London, England)* 10(12), 1911-22.

Savio, M., Stivala, L. A., Bianchi, L., Vannini, V., and Prosperi, E. (1998). Involvement of the proliferating cell nuclear antigen (PCNA) in DNA repair induced by alkylating agents and oxidative damage in human fibroblasts. *Carcinogenesis* 19(4), 591-6.

Sherman, M. H., Bassing, C. H., and Teitell, M. A. (2011). DNA damage response regulates cell differentiation. *Trends Cell Biol.* 21(5), 312-319.

Sikorski, R. S., Michaud, W. A., and Hieter, P. (1993). p62cdc23 of Saccharomyces cerevisiae: a nuclear tetratricopeptide repeat protein with two mutable domains. *Mol. Cell. Biol.* 13(2), 1212-1221.

Singh, N. P., McCoy, M. T., Tice, R. R., and Schneider, E. L. (1988). A simple technique for quantitation of low levels of DNA damage in individual cells. *Exp Cell Res* 175(1), 184-91.

Song, Y. H. (2005). Drosophila melanogaster: a model for the study of DNA damage checkpoint response. *Mol Cells* 19(2), 167-79.

Stergiou, L., and Hengartner, M. O. (2004). Death and more: DNA damage response pathways in the nematode C. elegans. *Cell Death Differ.* 11(1), 21-8.

Stevens, A.-S., Willems, M., Plusquin, M., Ploem, J.-P., Winckelmans, E., Artois, T., and Smeets, K. (2017). Stem cell proliferation patterns as an alternative for in vivo prediction and discrimination of carcinogenic compounds. *Sci. Rep.* 7, 45616.

Sugitani, N., Sivley, R. M., Perry, K. E., Capra, J. A., and Chazin, W. J. (2016). XPA: A key scaffold for human nucleotide excision repair. *DNA Repair* 44, 123-135.

Team (2013). RDC. R: a language and environment for statistical computing. *R foundation for statistical computing, Vienna, Austria*.

Udroiu, I., and Sgura, A. (2016). Genotoxic sensitivity of the developing hematopoietic system. *Mutation research. Reviews in mutation research* 767, 1-7.

Untergasser, A., Cutcutache, I., Koressaar, T., Ye, J., Faircloth, B. C., Remm, M., and Rozen, S. G. (2012). Primer3--new capabilities and interfaces. *Nucleic Acids Res* 40(15), e115.

van Wolfswinkel, J. C., Wagner, D. E., and Reddien, P. W. (2014). Single-cell analysis reveals functionally distinct classes within the planarian stem cell compartment. *Cell Stem Cell* 15(3), 326-39.

Vitale, I., Manic, G., De Maria, R., Kroemer, G., and Galluzzi, L. (2017). DNA Damage in Stem Cells. *Mol Cell* 66(3), 306-319.

Wagner, D. E., Wang, I. E., and Reddien, P. W. (2011). Clonogenic neoblasts are pluripotent adult stem cells that underlie planarian regeneration. *Science (New York, N.Y.)* 332(6031), 811-6.

Wyles, S. P., Brandt, E. B., and Nelson, T. J. (2014). Stem Cells: The Pursuit of Genomic Stability. *International journal of molecular sciences* 15(11), 20948-20967.

Zhang, C., Kong, D., Tan, M.-H., Pappas Jr, D. L., Wang, P.-F., Chen, J., Farber, L., Zhang, N., Koo, H.-M., Weinreich, M.*, et al.* (2006). Parafibromin inhibits cancer cell growth and causes G1 phase arrest. *Biochem. Biophys. Res. Commun.* 350(1), 17-24.

Zhang, L., Rahbari, R., He, M., and Kebebew, E. (2011). CDC23 regulates cancer cell phenotype and is overexpressed in papillary thyroid cancer. *Endocr. Relat. Cancer* 18(6), 731-42.

Zhu, S. J., and Pearson, B. J. (2016). (Neo)blast from the past: new insights into planarian stem cell lineages. *Curr. Opin. Genet. Dev.* 40, 74-80.

Figure legends

Fig. 1: DNA damage after MMS exposure. DNA damage in homeostatic (H) and regenerating (R) organisms after short (3 days) and long-term (17 days) exposure to 0 (control) or 50 µM MMS was assessed by the comet assay and expressed as the average of median % tail DNA. The values indicated in the graphs are the average ± standard errors of minimum 4 biological repeats from 2 independent experiments

(filtered suspension consisting of 10 organisms/sample). Significance, as compared to the corresponding H and R control group per exposure time, is indicated by ***: p-value < 0.01.

Fig. 2: Damage transducer (*smg1*) and effector (*p53*) responses to MMS. (a) Gene expression levels of the damage transducer *smg1* and the damage effector *p53* in homeostatic (H) and regenerating (R) animals after short (3 days) and long-term (17 days) exposure to 0 (control) or 50 µM MMS. Transcript levels are expressed relative to control homeostatic animals (expression level = 1). The values indicated in the graphs are the average ± standard errors of minimum 5 biological repeats. Significant effects, as compared to the corresponding control group per exposure time, are indicated by the following symbols:*** : p-value < 0.01;** p-value < 0.05. A significant main effect of MMS was found for *smg1* on the long term (p-value < 0.01). A significant main effect of regeneration for *p53* (p-value < 0.01) and *smg1* (p-value < 0.05) on the long term and for both genes an interaction effect (MMS*regeneration, p-value < 0.05 for *p53* and p-value < 0.01 for *smg1*) on the short term. (b) Phenotypic effects of *smg1* knockdown in regenerating animals (heads and tails) exposed to 0 (control) and 50 µM MMS following long-term (17 days) exposure in comparison with phenotypes of water-injected, unexposed and MMS-exposed regenerating animals. A minimum of 5 replicates per group was used as indicated in the figure.

Fig. 3: Cell cycle progression and proliferative responses following MMS exposure. Effects on cell cycle progression were investigated in homeostatic (H) and regenerating (R) animals after short (3 days) and long-term (17 days) exposure to 0 (control) or 50 µM MMS to compare (a) the number of mitotic cells per mm² measured by H3-mitotic staining. The values indicated in the graph are the average ± standard errors of minimum 4 biological replicates. Significant effects, as compared

to the corresponding H and R control group per exposure time, are indicated by the following symbols; *** : p-value <0.01; **: p-value <0.05. An interaction effect between MMS treatment and regeneration was found on the long-term (p-value < 0.01). (b) Relative expression of the cell cycle regulators *cdc23* and *cdc73*. Measurements are expressed relative to control homeostatic animals (expression level = 1). The average ± standard errors of minimum 5 replicates are shown. On the long term, a main effect of MMS was observed for *cdc23* (p-value < 0.05); a regeneration effect for *cdc73* (p-value < 0.05). (c) *smedwi-1* levels in regenerating animals measured with WISH. A minimum of 6 biological replicates for each condition was used as indicated in the figure. Scale bar represents 500 µm. (d) *Smedwi-1* FISH on regenerating tails following 2 days of exposure. One confocal stack is shown. Scale bar represents 200 µm. (e) Heatmap representing log10 transformed relative gene expression levels of a selection of sigma-related genes (*soxP-1, soxP-2, fgfr-4, soxB-1, nlk-1, pbx-1)* and a selection of zeta-related genes (*zfp-1*, *soxP-3*, *fgfr-1* and *p53*) following long-term (17 days) exposure to 50 µM MMS. Six biological replicates were used per experimental condition, missing values are depicted in grey.

Fig. 4: Effect of MMS exposure on stem cell differentiation processes. (a) *NB.21.11e* (early progeny marker) WISH in regenerating head, trunk and tail parts after short (3 days) and long-term (17 days) exposure to 0 (control) or 50 µM MMS. Scale bar represents 500 µm. Minimal 6 biological replicates per condition were used, as indicated in the figure. (b) Gene expression measurements of *NB32.1g* (early progeny marker) and *agat-1* (late progeny marker), expressed relative to control homeostatic animals (expression level = 1). The averages +/- standard errors of minimum 5 biological replicates are shown. Significant effects, as compared to the corresponding H and R control group per exposure time, are indicated by the

following symbol *** : p- value <0.01. An interaction effect between treatment and regeneration was significant (p-value < 0.05) for *NB.32.1g* on the short term; a main effect of regeneration on the long-term for *AGAT-1* (p-value < 0.05). (c) SMEDWI-1 protein levels in regenerating heads and tails after short-term (3 days) exposure to 0 (control) or 50 µM MMS. The blastema (i.e. region where new tissue is developing) is depicted. Minimum 4 biological replicates were used as indicated in the figure. Scale bar represents 200 µm.

Fig. 5: Apoptosis in response to MMS. Apoptosis was investigated in homeostatic (H) and regenerating (R) animals after short (3 days) and long-term (17 days) exposure to 0 (control) or 50 µM MMS. (a) The number of apoptotic cells per mm^2 measured by a TUNEL assay. The average ± standard errors of minimum 3 replicates is depicted. A main effect of regeneration was significant on the short term (p-value < 0.05). (b) Gene expression levels of a proapoptotic *bcl-2* antagonist and the prosurvival *bcl-2* gene. Gene expression data are represented relative to control homeostatic animals (expression level = 1). Significant effects, as compared to the corresponding H or R control group per exposure time are indicated by the following symbols ***: p-value <0.01;** : p-value <0.05,* : p-value <0.1. A main effect of regeneration was significant for *bcl-2* antagonist on the long term (p-value < 0.01).The values indicated in the graphs are the averages ± standard errors of minimum 5 biological replicates.(c) Mitotic divisions per mm^2 after long-term MMS exposure in regenerating animals with or without RNAi knockdown of a *bcl-2* antagonist. The number of mitotic cells was normalized against the total body area of the worms and expressed relative to the non-exposed, non-RNAi group which was injected with water. The average and standard error of the non-RNAi control group is 159.5 ± 12.8 cells/mm^2. The average ± standard errors of minimum of 4 biological repeats is depicted.

Fig. 6:DNA repair in response to MMS. DNA repair was assessed in homeostatic (H) and regenerating (R) animals after short (3 days) and long-term (17 days) exposure to 0 (control) or 50 µM MMS. (a) Gene expression levels of *ku70, ku80* (non-homologous end-joining) and *pcna* (base excision repair). Gene expression levels are represented relative to control homeostatic animals (expression level = 1). The values indicated in the graphs are the averages ± standard errors of minimum 4 biological replicates. Significant effects, as compared to the corresponding H or R control group per exposure time are indicated by the following symbols: *** p-value <0.01;** : p-value <0.05,* p-value <0.1. For *ku70*, there was a significant interaction effect on the short term (p-value < 0.05) and a regeneration effect on the long term (p-value < 0.05). For *pcna*, a regeneration effect was significant on the short term (p-value < 0.01). (b) Phenotypic effect of *pcna*, *rad51* or *ku80* knockdown in combination with long-term (17 days) 50 µM MMS exposure. Control animals were injected with water. Minimum 6 biological replicates per group were used as indicated in the figure. *Rad51* knockdown heads exposed to MMS died prematurely (represented by a cross). (c) Mitotic divisions per mm^2 after long-term MMS exposure (17 or 18 days) in regenerating animals with or without RNAi knockdown of *pcna* or *rad51* of minimal 4 (*rad51*, tail fragments) or 5 (*pcna*) biological replicates per group. The number of mitotic cells is expressed relative to the non-exposed, non-RNAi group (which had a value of 107.6 ± 10.8 cells/mm^2 in case of the *pcna* experiment and 163.2 ±27 cells/mm^2 for the *rad51* experiment). Significant effects, as compared to the corresponding R control group per exposure time are indicated by: *** : p-value < 0.01. A main effect of *pcna* knockdown and an interaction effect between knockdown and treatment were significant (p-value < 0.01) for the *pcna* knockdown experiment. For *rad51* knockdown, main effects of treatment and regeneration as

well as their interaction were significant (p-value < 0.05). (d) PCA analysis of DNA repair, apoptotic and sigma/zeta subclass-associated genes following long-term exposure to 50 µM MMS in regenerating animals. PCA was performed on the gene expression data of the same samples as Fig. 5b and 6a with the addition of a selection of sigma-associated genes (*soxP-1, soxP-2, fgfr-4, nlk-1, pbx-1, soxB-1)* and a selection of zeta-associated genes (*soxP-3, fgfr-1, p53* and *zfp-1*). Each dot represents a gene, colours indicate to which class it belongs with sigma (pink), zeta (light blue), repair (red), and apoptosis (blue).(e) Heatmap representing the log10 value of relative gene expression levels of sigma-associated genes (*soxP-1* and *soxP-2*) and the zeta-exclusive gene *zfp-1* measured on a stem cell-containing fraction, isolated following 10 days of 50 µM MMS exposure in combination with *rad51* or *pcna* knockdown in regenerating head fragments. Control animals were injected with water (H_2O group). The inner circle represents control groups, the outer circle MMS-treated animals. At least 5 biological replicates (consisting of 6 animals per sample) per experimental group were measured with missing values depicted in grey.

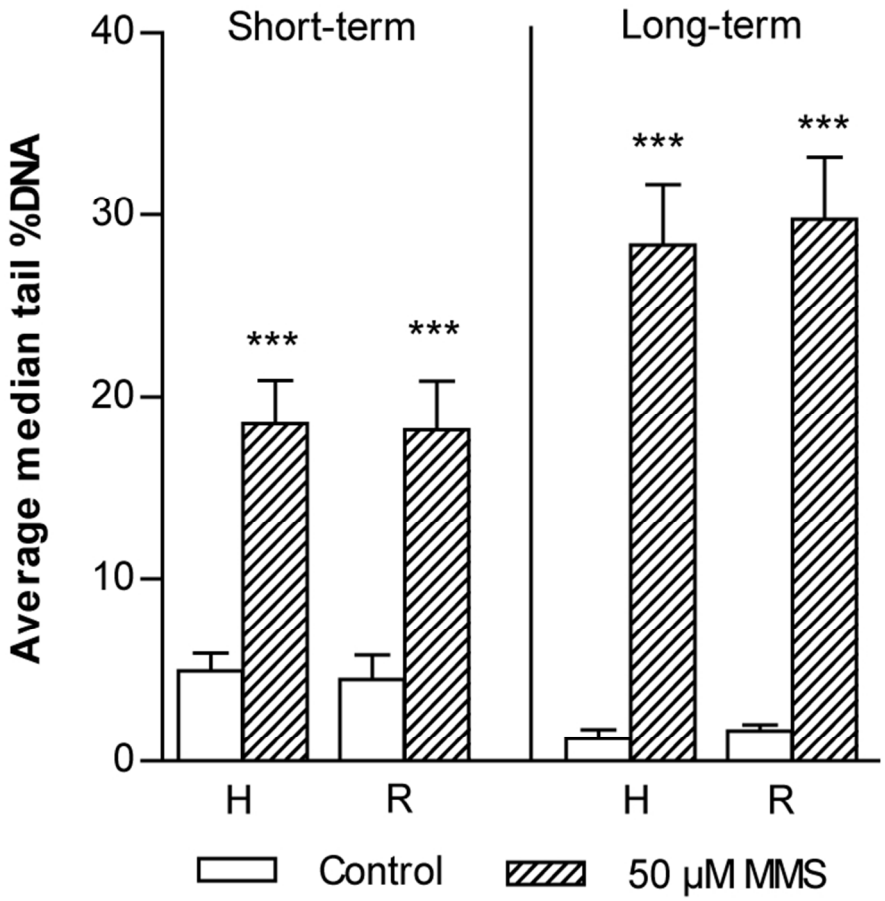

Figure 1

69x67mm (300 x 300 DPI)

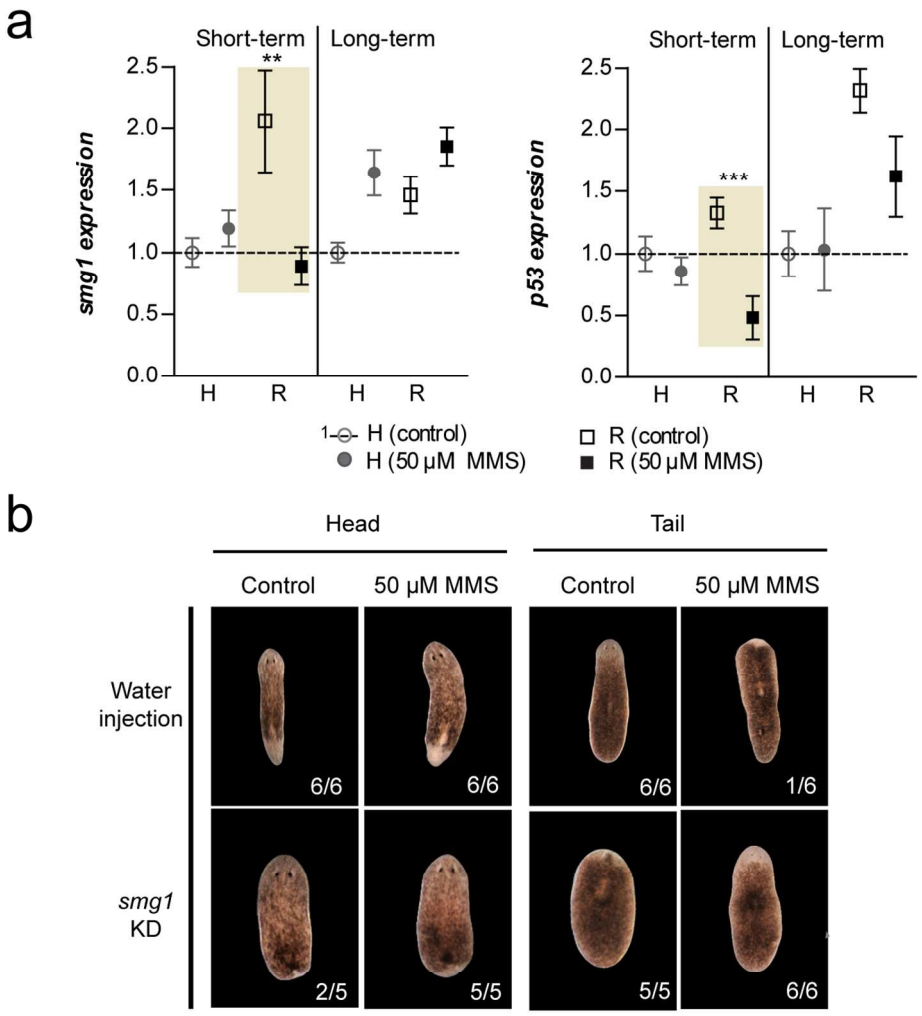

Figure 2

122x133mm (300 x 300 DPI)

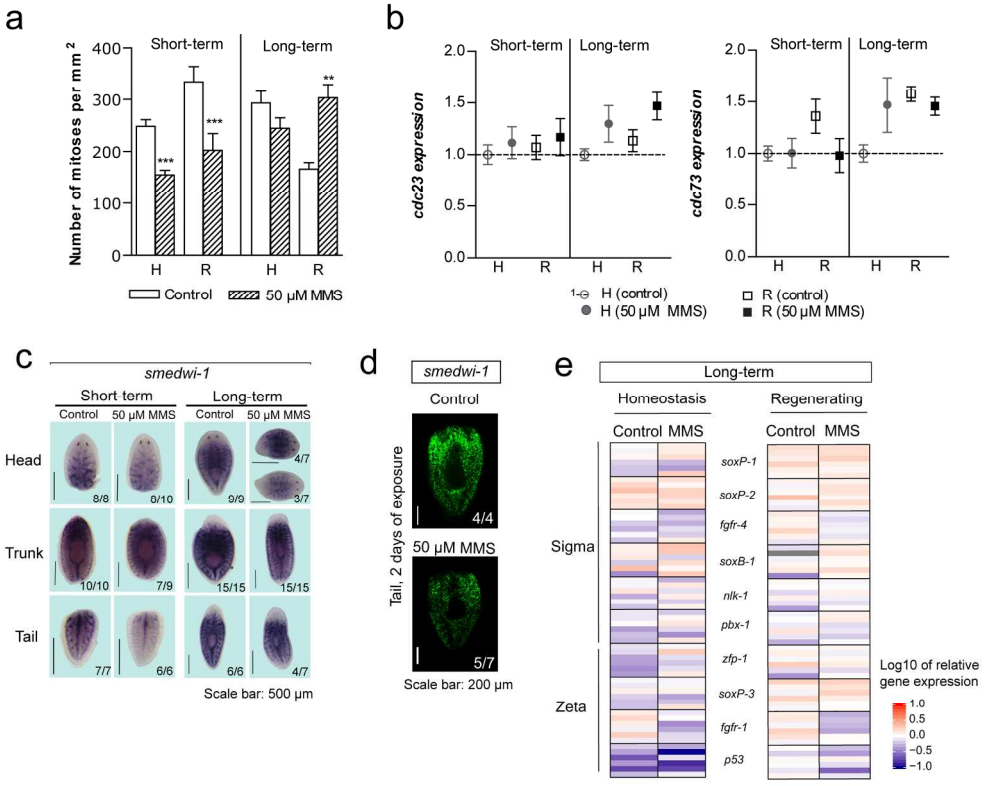

Figure 3

183x149mm (300 x 300 DPI)

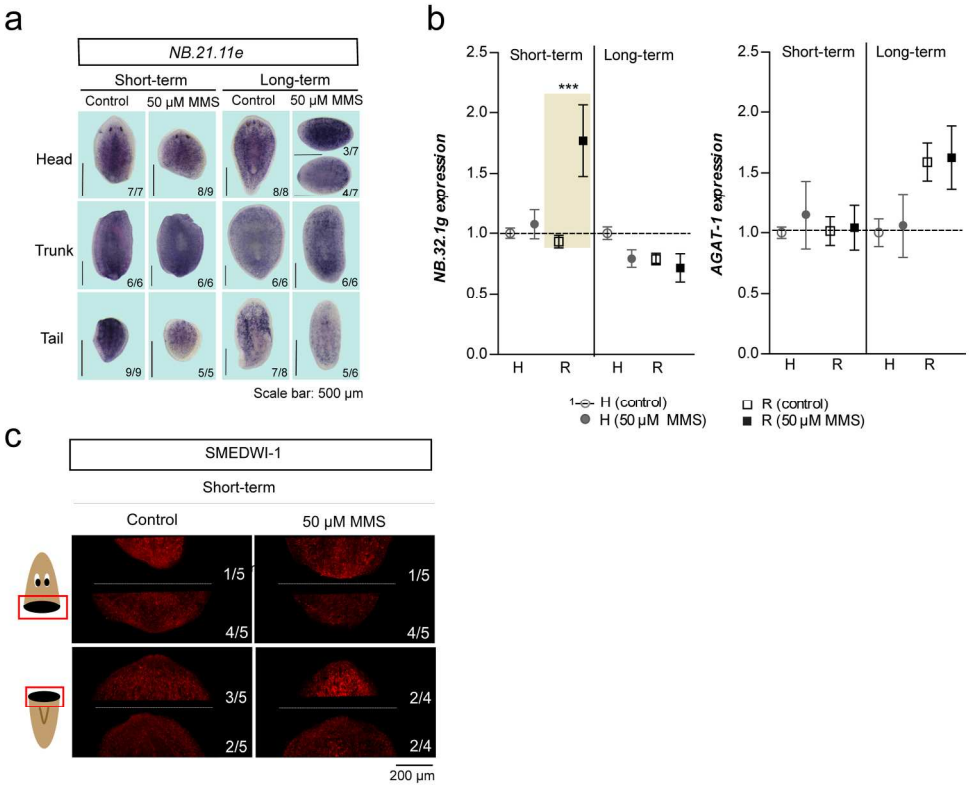

Figure 4

183x149mm (300 x 300 DPI)

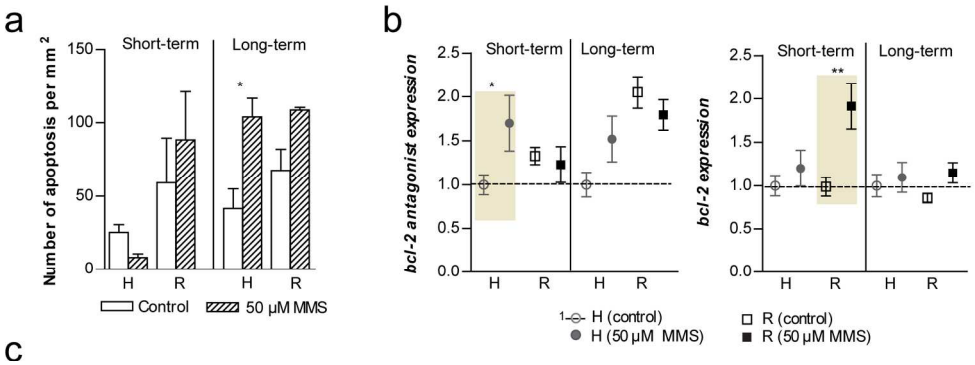

c

Mitotic division

	Control	50 µM MMS	
water	1	1.59 ± 0.30	**
bcl-2 antagonist	0.97 ± 0.15	1.54 ± 0.11	*

Figure 5

173x96mm (300 x 300 DPI)

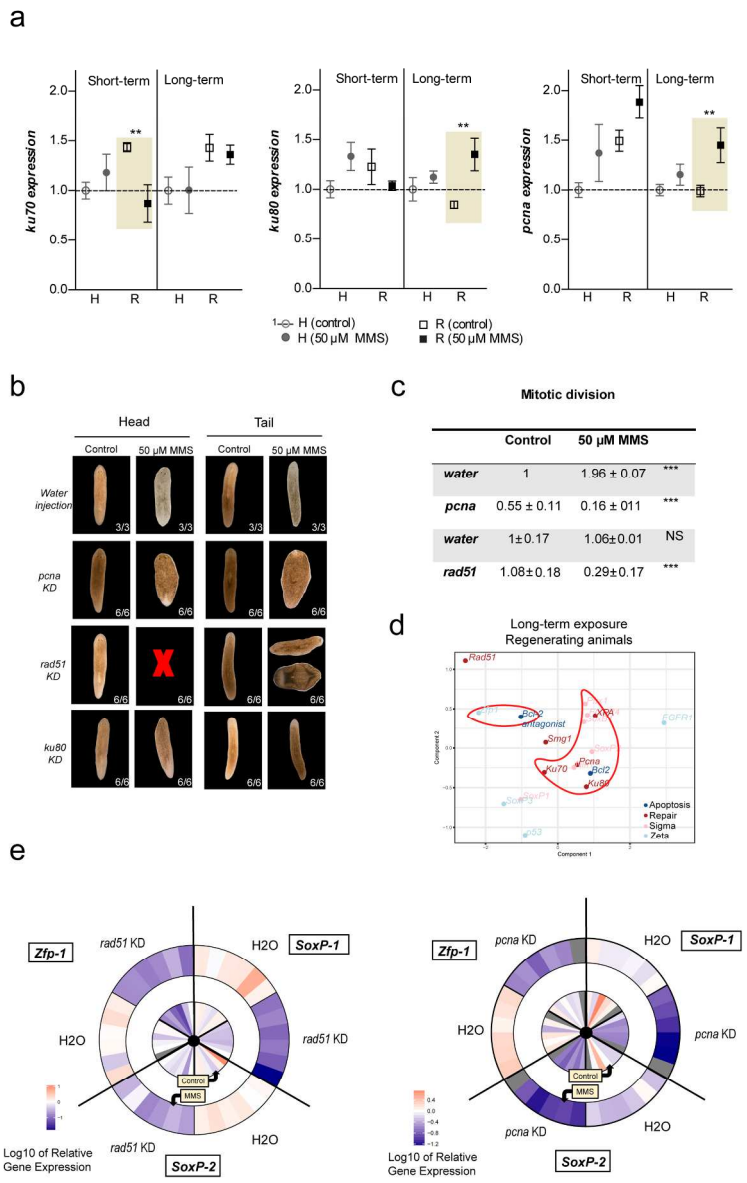

Figure 6

186x258mm (300 x 300 DPI)